Effect of structural evolution and surface morphological changes on the electrochemical response of an FeNbAlMnCuSiB alloy

A. K. PANDA
National Metallurgical Laboratory, Jamshedpur 831 007 India

M. MANIMARAN
3 Research Link, IMRE, Singapore 117602

S. BASU
Materials Science Centre,Indian Institute of Technology, Kharagpur 721 302

A. MITRA, I. CHATTORAJ*
National Metallurgical Laboratory, Jamshedpur 831 007 India
E-mail: ichatt_62@yahoo.com

The electrochemical response of a soft magnetic FeNbAlMnCuSiB alloy was studied through different stages of devitrification. The structural evolution including appearance of a nanocrystalline phase and intermetallics, and accompanying surface topographical changes were studied and correlated to the electrochemical behavior of this alloy. The electrochemical behavior was not directly related to changes in surface roughness but it was very responsive to the structural changes, particularly to the formation of the nanocrystalline phase and to the precipitation of Fe_7Nb_6 phase. There was a progressive passivation breakdown with the appearance of crystalline phases on annealing.

1. Introduction

Amorphous alloys owe their good corrosion resistance to their chemical homogeneity. In these alloys the absence of precipitates and grain boundaries contribute towards their high corrosion resistance [1]. The Fe-metalloid based amorphous alloys exhibit higher corrosion resistance than their crystalline counterparts [2, 3]. The corrosion resistance of these amorphous alloys are reported to be increased by the presence of additional elements like Nb [4]. Besides Nb, the metalloids Si and B have been found to affect the corrosion behaviour in Fe-Si-B amorphous systems where Si is reported to be less deleterious than B [5, 6].

Besides the corrosion behavior, the alloying effects of Nb, Si, B and Cu have their utmost significance in the ultra-soft magnetic properties of the Fe-Nb-Cu-Si-B [7] based nanocrystalline alloy, also known as FINEMET. All these elements play a key role in the nanocrystallization mechanism where Cu serves as a nucleation centre for α-Fe(Si) nanoparticles while the element Nb impedes their growth [8]. The element B along with Si acts as a stabiliser of the amorphous precursor. Although the role of these elements on electrochemical corrosion property of the amorphous alloys has been investigated, there are only few reports on their effect in the FeNbCuSiB system [9–11] which have tremendous potential as sensor materials. Further more, the fact that corrosion being a surface phenomena, and evidences suggesting the formation of crystallites more easily in the surface than within the bulk [12, 13], there is a need to investigate the associated surface morphological developments in these materials.

The present investigation addresses the corrosion behavior with structural changes and surface morphological changes in as-cast and heat-treated soft magnetic FeNbAlMnCuSiB alloy, which has been found to have different and in some respects better magnetic properties than the well-known FINEMET [14]. To the best of our knowledge the electrochemical behavior of this multi-component alloy has not been reported.

2. Experimental

The alloy in the form of ribbons having a nominal composition of $Fe_{71}Nb_{3.7}Cu_1Al_3Mn_{0.8}Si_{13.5}B_7$ was prepared by melt spinning at National Metallurgical Laboratory. The ribbons were annealed for 30 min at predetermined temperatures in vacuum (10^{-2} Torr). The electrochemical corrosion studies of as-cast and heat-treated alloys were carried out in a buffered

*Author to whom all correspondence should be addressed.
0022-2461
DOI: 10.1007/s10853-005-0921-3

TABLE I Phase evolution with anealing

Annealing* temperature (K)	Phases present	Particle size of the predominant phase (nm)
As cast	Amorphous	–
800	Fe_3Si/α-Fe(Si, Al)	6 ± 0.3
825	Fe_3Si/α-Fe(Si, Al), $Fe_{23}B_6$	8.2 ± 0.4
875	Fe_3Si/α-Fe(Si, Al), $Fe_{23}B_6$	10.7 ± 0.5
925	Fe_3Si/α-Fe(Si, Al), $Fe_{23}B_6$	11.0 ± 0.5
975	Fe_3Si/α-Fe(Si, Al), $Fe_{23}B_6$, Fe_2B, Fe_7Nb_6	Completely crystallised

*Annealed for 30 min in vacuum.

chloride solution. A 0.1 M acetate buffer was prepared by mixing sodium acetate and acetic acid in distilled water. Sodium chloride was added to the buffer to produce halide concentrations of 0.01 M and 1 M. The electrochemical behavior was measured by potentiodynamic tests using a potentiostat. A platinum counter electrode and a saturated calomel reference electrode (SCE) were used. The ribbon sample acted as the working electrode. In the potentiodynamic tests, the alloys were scanned at the rate of 0.5 mV/sec, starting from a negative (cathode) overpotential and ending at a suitable positive (anodic) overpotential. The scan rate chosen was slow enough to reveal passivation if it occurred.

Phase evaluation of the as prepared and heat treated alloys was done using X-ray diffractometry (XRD). Microstructural studies were done by Transmission electron microscopy, (TEM). The evolution of surface morphology of the samples with heat treatment was studied ex-situ by an Atomic Force Microscope (AFM).

3. Results and discussions

3.1. Structural evolution

The evolution of the crystalline phases in the amorphous matrix was revealed through XRD peaks after annealing at certain critical temperatures. This was discussed in detail elsewhere [14]. The crystallization onset temperature of this alloy had been determined by TEM observations in the Selected Area Diffraction mode to be around 775 K while the less sensitive Differential Scanning Calorimetry as well as electrical resistivity measurements indicated the crystallization temperature to be around 800 K. Annealing at 800 K produced the nanocrystalline phase. This was either a superlattice compound Fe_3(Si, Al) or a solid solution conforming to α-Fe (Si, Al). Lattice parameter measurements showed that it was close to but different from that for Fe_3Si. The best soft magnetic property was also observed on annealing at 800 K, which corresponds to a microstructure of nanocrystalline phases distributed in an amorphous matrix. Further annealing caused the appearance of $Fe_{23}B_6$ phase at 825 K. The Fe_2B phase is reported to form at elevated temperatures beyond 875 K [15]. The strong magnetocrystalline anisotropy of this phase is detrimental towards soft magnetic properties [16]. However, this phase is detectable only after annealing at 975 K for the alloy studied, and in minor amounts. An additional Fe_7Nb_6 phase appeared on annealing at 975 K, along with minor amounts of Fe_2B.

3.2. Surface morphology evolution

In the FeNbCuSiB based systems the low solubility of Cu in Fe (<0.2 at%) leads to its early partitioning on annealing. In metallic glasses such partitioning are observed in slow quenched as-cast materials [17]. The first stages of crystallization were observed by AFM studies of Fe-Si-B alloys [18]. In the present study the surface topography of the samples was observed to change with annealing. The as-received samples had a high roughness; roughness here refers to microscale roughness and not the macroscale roughness that is inherent to ribbons due to the process of melt-spinning. The change in surface topography is shown in Fig. 1 for three different annealing treatments. The height as well as the shape and diameter of the protrusions change with annealing as is evident in the figure. The initial sharp, tall protrusions of the amorphous alloys (Fig. 1a) change into more rounded shapes and become shorter on annealing at the crystallisation onset temperature (Fig. 1b). There is the appearance of "double-humps", which according to Watanabe *et al.* [18] is indication of pre-crystallisation seeding or nucleation, and in this case is possibly caused by Cu segregation. On annealing at a higher temperature of 875 K (Fig. 1c) these double humped protrusions grow and their height as well as girth increases—this possibly corresponds to the growth of the crystallites. The variation of roughness (root mean square (RMS) value) with annealing is shown in Fig. 2. On progressive annealing the surface roughness goes through a minimum, interestingly this minimum corresponds to the appearance of the nanocrystalline phase and consequent excellent soft magnetic properties.

3.3. Electrochemical response

Potentiodynamic studies were carried out for the as-cast and different heat-treated samples in the chloride media. Figs 3 and 4 show the electrochemical responses of the alloy during different stages of devitrification, in two different chloride media. The as-cast sample exhibits passivity over almost the entire anodic range tested in the 0.01 N chloride containing buffer (Fig. 3). The detrimental effect of chloride concentration on the passivation of the amorphous alloys may be seen from the much-reduced passive regime in 1N chloride concentration: the passive breakdown is quite abrupt (Fig. 4). For this alloy, the amorphous as-received state is most resistant to corrosion in both the chloride concentrations which is contrary to the findings for certain FeBSiNbCu alloys [9] where the appearance of the nanocrystalline phase was found to be beneficial. In this alloy there is a progressive deterioration of corrosion resistance with annealing, at pre-crystallization as

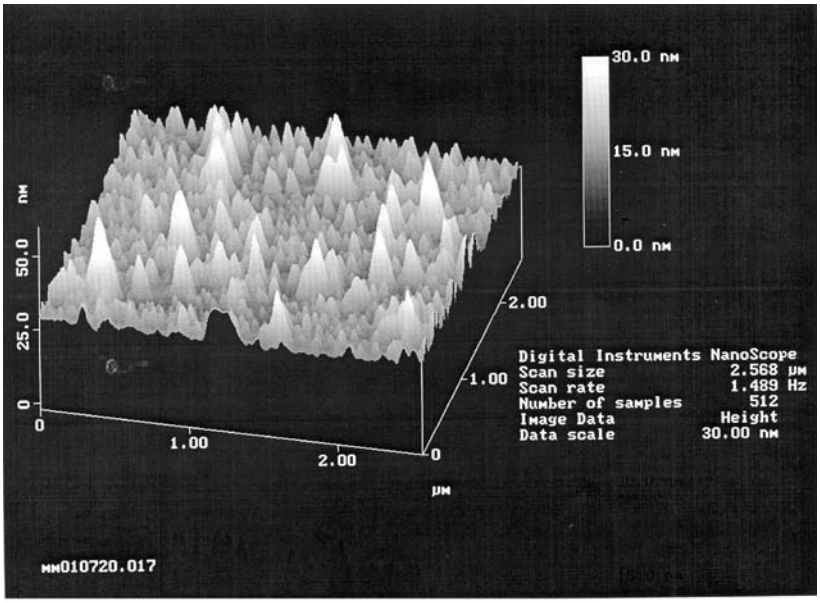

(a)

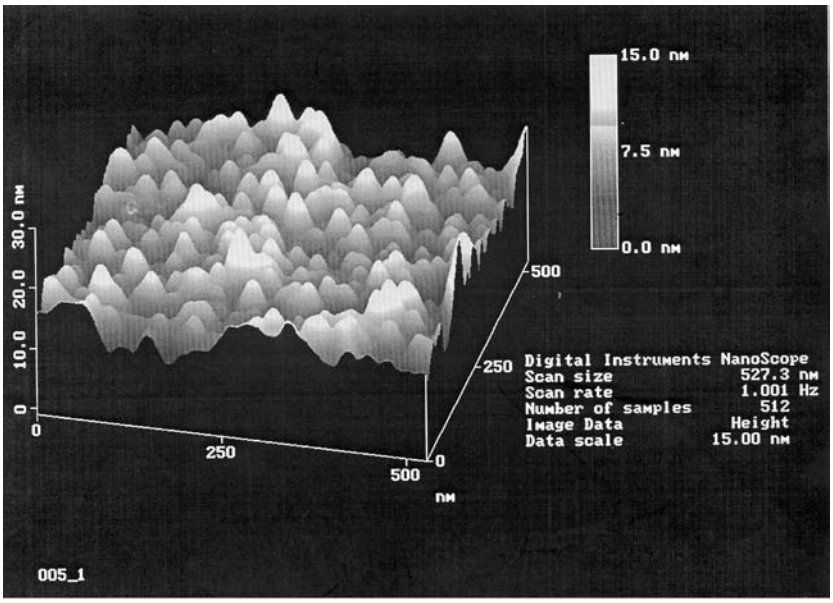

(b)

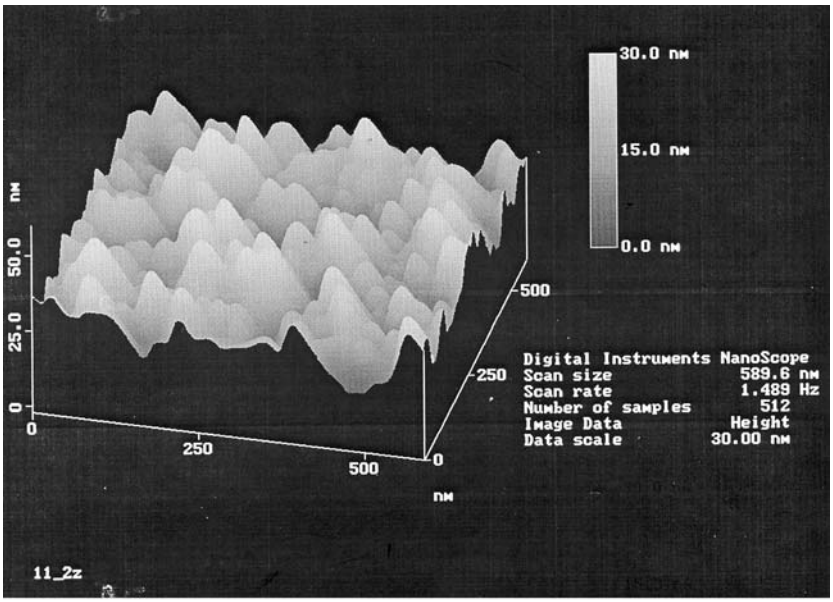

(c)

Figure 1 AFM observation of the surface roughness in differently annealed samples (a) as-cast samples; (b) annealed at 775 K; and (c) annealed at 875 K.

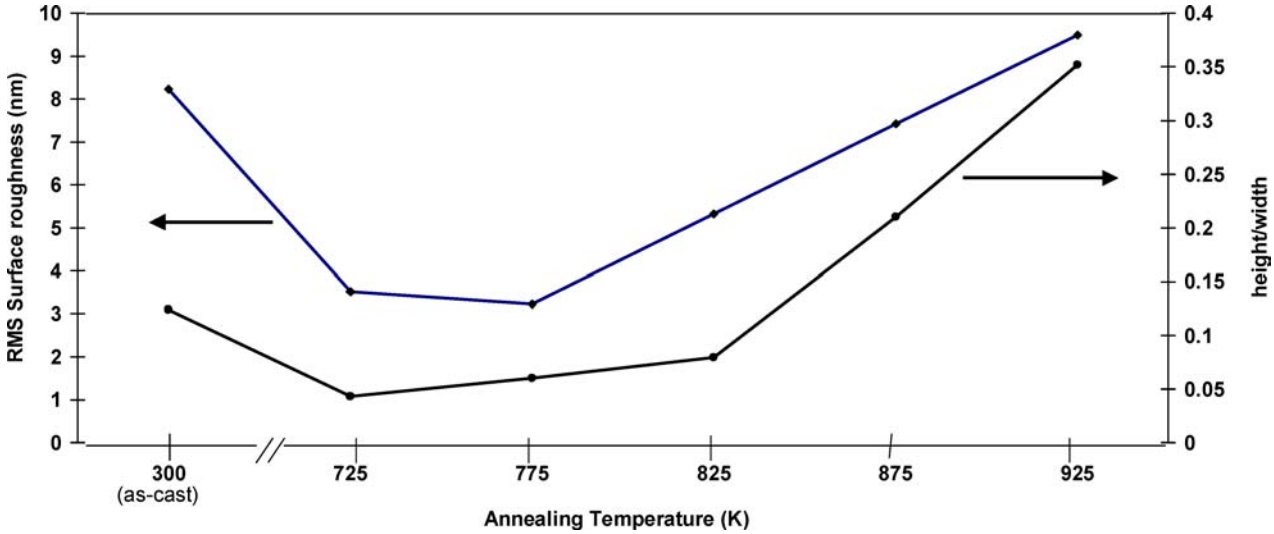

Figure 2 The variation in surface topography with annealing.

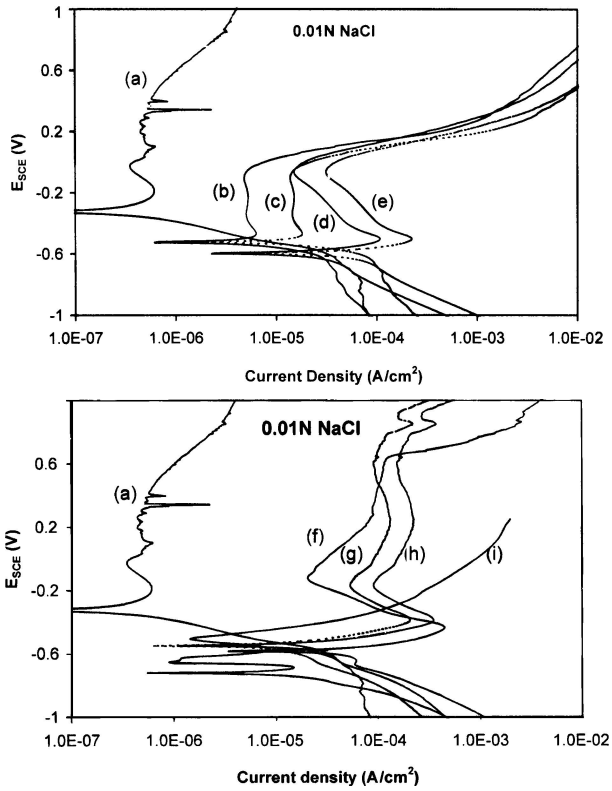

Figure 3 Potentiodynamic polarisation in acetate buffer containing 0.01 M NaCl for different heat treated samples: (a) as-cast; (b) and (c) annealed at 725 K; (d) and (e) annealed at 775 K; (f) annealed at 825 K; (g) and (h) annealed at 875 K; (i) annealed at 975 K; (c), (e) and (g) are for normalised surface roughness.

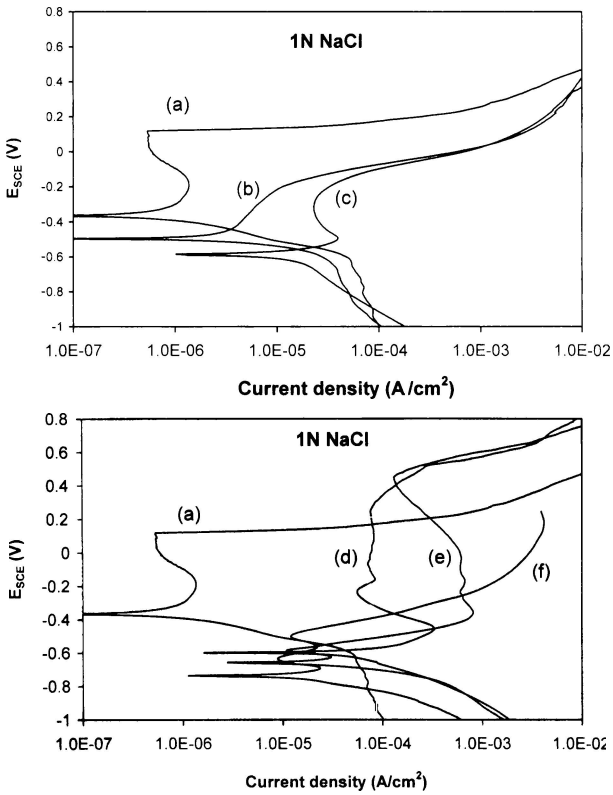

Figure 4 Potentiodynamic polarisation in acetate buffer containing 1 M NaCl: (a) as-cast; (b) annealed at 725 K; (c) annealed at 775 K; (d) annealed at 825 K; (e) annealed at 875 K; (f) annealed at 975 K.

well as at post-crystallization temperatures. Passivity is exhibited by the samples annealed below crystallization temperature, at 725 K, and those annealed just at the crystallization temperature (775 K), but the extent (potential range) of the passivity is much reduced. Interestingly, the samples annealed at 825 and 875 K showed apparent passivity in both media, but with a higher passive current density. Thus the appearance of the nanocrystalline phase does impart some protection to this alloy too. Annealing at a higher temperature (975 K) resulted in substantial loss of corrosion resistance and total absence of any passivation in either media.

The electrochemical response has to be analyzed with respect to the structural and surface morphological changes occurring in the material. If we consider surface changes, one obvious effect is the surface area effect. It is evident from Fig. 2. that the as-cast samples had a high actual surface area. To accommodate for the topographical differences we normalized the surface roughness for the samples

with respect to that for the as-cast samples and expressed the current density in terms of the normalized surface area thus obtained. The polarization curves using the normalized surface area are shown for some samples in Figs 3a and b. Obviously the surface roughness was not a major factor in the electrochemical response of the alloys, that is, the annealing variations could not be explained by the surface topographical changes.

On the other hand, the electrochemical response was very susceptible to structural changes. Annealing near the crystallization temperature result in pre-crystallization seeding — this is seen to bring about a significant decrease of the corrosion resistance. The appearance of the nanocrystalline phase, however, did impart some corrosion resistance to the alloy. This can be seen by comparing the behavior of the samples annealed at 775, 825 and 875 K, which show an increasing proportion of the nanocrystalline $Fe_3(Si, Al)/\alpha$-Fe (Si, Al). In these cases there is a substantial passive regime, albeit with high passive current density (of the order of 100 $\mu A/cm^2$). The benefits of the nanocrystalline phase is not negated by the precipitation of $Fe_{23}B_6$ particles as is evident in the polarization behavior of the samples annealed at 825 K when this phase first appears as well as on its subsequent proliferation and growth at 875 K. The rapid loss of corrosion resistance on annealing at 975 K is coincident with the appearance of the Fe_7Nb_6 phase. The appearance of Fe_2B at this annealing temperature is relatively minor, and B loss from the amorphous matrix occurs more due to the formation of $Fe_{23}B_6$. However, the electrochemical response at all stages after crystallization has to be viewed keeping in mind several other important structural changes which occur at higher temperatures. These are, a progressive decrease in the amorphous phase fraction, a conversion of nanocrystalline phase to microcrystalline proportions through growth, profuse intermetallic precipitation ($Fe_{23}B_6$ and Fe_7Nb_6) and a change in the amorphous phase composition through rejection of certain elements to the amorphous phase. The progressive crystallization of the alloy may be represented by the following schematic reaction based on mass conservation on the lines of Yavari's [19] proposal:

$$\begin{aligned} &Fe_{71}Nb_{3.7}Cu_1Al_3Mn_{0.8}Si_{13.5}B_7 \\ &\rightarrow \underset{\text{(nanocrystalline)}}{0.675Fe_{80}(SiAl_{0.22})_{20}} \\ &+ \underset{\text{(amorphous matrix)}}{0.325Fe_{52.3}B_{21.5}Mn_{2.46}Nb_{11.4}} + Cu \qquad (1) \end{aligned}$$

Where $Fe_{80}(SiAl_{0.22})_{20}$ is the nanocrystalline phase that first appears and is surrounded by an amorphous matrix which is rich in B, Mn and Nb which are rejected by the nanocrystalline phase. The amorphous matrix progressively gets richer in these elements with the above reaction setting the theoretical limits for the enrichment of these elements. However, at higher temperatures, the amorphous matrix also suffers dissociation due to the formation of, first, the $Fe_{23}B_6$ precipitates, and later, the Fe_7Nb_6 precipitates and Fe_2B precipitates. Thus the loss of corrosion resistance should be viewed as a culmination of all these effects. It may be noted that the precipitation of $Fe_{23}B_6$ did not seem to have much of an effect on the corrosion resistance, while apparently the precipitation of Fe_7Nb_6 was accompanied by a rapid loss of resistance. While keeping in mind that the electrochemical response is affected by a number of structural changes, this observation does inferentially support the findings of some authors that Nb in the amorphous matrix is beneficial while B is not.

4. Conclusions

The effect of heat-treatment on the structural evolution and surface morphological changes and consequent effects on the electrochemical behavior of $Fe_{71}Nb_{3.7}Cu_1Al_3Mn_{0.8}Si_{13.5}B_7$ alloy was investigated. It was observed that the surface roughness changed with annealing going through a minimum near the crystallisation temperature. The electrochemical behavior was not directly related to changes in surface roughness, this was verified by using a normalised surface area in the electrochemical current density calculations. The electrochemical behavior was very responsive to the structural changes, particularly to the formation of the nanocrystalline phase and to the precipitation of Fe_7Nb_6 phase. The appearance of Fe_2B at this annealing temperature is relatively minor. The passivation current systematically increased with annealing temperature indicating passivation breakdown. The best corrosion response was observed in the as-cast material. Crystallisation caused a decrease in the corrosion resistance; however, the presence of, and increase in, nanocrystalline phase content did provide corrosion resistance to some extent corroborating earlier observations in FINEMET alloys [9].

References

1. M. NAKA, K. HASHIMOTO and T. MASUMOTO, J. Japan Inst. Metals **38** (1974) 835.
2. M. NAKA, K. HASHIMOTO, T. MASUMOTO and A. INOUE, *J. Non-cryst. Sol* **31** (1979) 347.
3. P. CADET, M. KEDDAM and H. TAKENOUTI, in Proceedings of 4th International Conference on Rapidly Quenched Metals, Sendai, 1982, p. 1447.
4. Y. WASEDA and K. T. AUST, *J. Mater. Sci.* **16**(1981) 2337.
5. U. LINKER and W. J. PLIETH, in Proceedings of 5th International Conference on Rapidly Quenched Metals, Wurzburg (1984) p. 1465.
6. K. HASHIMOTO, K. KOBAYASHI, K. ASAMI and T. MASUMOTO, in Proceedings of 8th International Congress on Metallic Corrosion, Frankfurt/Main (1981) p. 70.
7. Y. YOSHIZAWA, S. OGUMA, K. YAMAUCHI, *J. Appl. Phys.* **64** (1988) 6044.
8. Y. YOSHIZAWA and K. YAMAUCHI, *Mater. Trans. JIM*, **31** (1990) 307.
9. I. CHATTORAJ, K. RAM MOHAN RAO, S. DAS and A. MITRA, *Corros. Sci.* **41** (1999) 1.
10. I. CHATTORAJ and A. MITRA, *Scripta Mater.* **39** (1998) 755.
11. C. A. C. SOUZA, S. E. KURI, F. S. POLITTI, J. E. MAY and C. S. KIMINAMI, *J. Non-cryst. Sol.* **247** (1999) 69.
12. U. KOSTER, *Mater. Sci. Eng.* **97** (1988) 233.
13. A. GUPTA and S. HABIBI, *ibid. A* **133** (1999) 375.

14. A. MITRA, A. K. PANDA, S. R. SINGH, V. RAO and P. RAMACHANDRAO, *Philos. Mag.* **83** (2003) 1495.
15. G. HERZER, in Handbook of Magnetic Materials, vol. 10 (Elsevier Science, B.V., 1997) p. 422.
16. T. KULIK and A. HERNANDO, *Mater. Sci. Forum.* **179** (1995) 587.
17. A. L. GREER, *J. Mater. Sci.* **17** (1982) 1117.
18. Y. WATANABE and Y. NAKAMURA, *J. Mater. Res.* **7** (1992) 2126.
19. A. R. YAVARI, in Proceedings of 4th International Workshop on Non-crystalline solids, Madrid (1994) p. 35.

Received 9 October 2004
and accepted 14 March 2005